

Technical Note

Analysis of Multipath Changes in the Polish Permanent GNSS Stations Network

Jacek Rapiński ^{1,*}, Dariusz Tomaszewski ^{1,†} and Renata Pelc-Mieczkowska ^{2,†}¹ Department of Geodesy, Faculty of Geoengineering, University of Warmia and Mazury in Olsztyn, 10-719 Olsztyn, Poland; dariusz.tomaszewski@uwm.edu.pl² Department of Geoinformation and Cartography, Faculty of Geoengineering, University of Warmia and Mazury in Olsztyn, 10-719 Olsztyn, Poland; renata.pelc@uwm.edu.pl* Correspondence: jacek.rapinski@uwm.edu.pl

† These authors contributed equally to this work.

Abstract: This study examines the influence of multipath errors on Global Navigation Satellite System (GNSS) measurements collected at ASG-EUPOS reference stations between 2010 and 2021. Multipath occurs when GNSS signals reflect off surrounding objects before reaching the receiver antenna, leading to positioning errors. In the case of reference stations, all available mitigation techniques were used to minimize the impact of multipath. However, it is still detectable and affects the measurement results. For carrier phase differential positioning, it increases the ambiguous search space, which results in a decrease in determining rover—reference station vector accuracy. The study employs two linear combinations (Code-Minus-Carrier and Multipath Pseudorange Observable) to quantify the multipath effect on both pseudorange and carrier phase measurements. Based on the research, it was found that the multipath values changed depending on the change of the receiver and the terrain around the reference stations. The study observed a gradual decrease in multipath errors from 2010 to 2021, likely due to technological advancements in receiver design. No significant increase in multipath errors was observed due to environmental changes around the stations, suggesting a minimal influence from new reflecting objects nearby. Based on the analyses conducted, it is also recommended to perform periodic tests to detect incorrect receiver configuration or operation.



Citation: Rapiński, J.; Tomaszewski, D.; Pelc-Mieczkowska, R. Analysis of Multipath Changes in the Polish Permanent GNSS Stations Network. *Remote Sens.* **2024**, *16*, 1617. <https://doi.org/10.3390/rs16091617>

Academic Editor: Yunbin Yuan

Received: 21 March 2024

Revised: 26 April 2024

Accepted: 29 April 2024

Published: 30 April 2024



Copyright: © 2024 by the authors. Licensee MDPI, Basel, Switzerland. This article is an open access article distributed under the terms and conditions of the Creative Commons Attribution (CC BY) license (<https://creativecommons.org/licenses/by/4.0/>).

1. Introduction

A single GNSS satellite signal covers a large area of the earth's surface. The receiver's antenna acquires only a small part of the broadcasted information. Naturally, the transmitted signal reflects off objects around the antenna. Some of these reflected signals also reach the receiver antenna. Eventually, the signal recorded by the device usually combines direct signals (LOS—Line-Of-Sight) and indirect signals (non-LOS). In an extreme case, the recorded signals may be from non-LOS signals only. Consequently, this results in measurement errors in both code and phase observables. The term multipath is used to describe the effect of the reflected signals on the loss of accuracy and reliability of the obtained position.

Due to its nature, multipath significantly impacts both absolute and differential positioning. However, the impact of this error on each measurement type is different [1]. In the case of pseudorange, the indirect signal interferes with the correlation of the direct signals' Pseudo Random Noise (PRN). As a result, the main peak of the autocorrelation function is deformed and does not reflect the code phase of the LOS wave, which directly affects the accuracy of the pseudorange measurement and may result in a loss of lock [2]. The size of the tracking error depends on the receiver/antenna design and the properties of the reflected signal [3]. Hofmann-Wellenhof et al. stated that non-LOS signals can cause errors in pseudorange determination up to 20 m [4]. In the case of carrier phase measurement,

the maximum tracking error resulting from the multipath phenomenon is a quarter of the carrier wavelength [5,6]. Therefore, for GPS satellites, this value will be approximately 4.8 cm, 6.0 cm, or 6.4 cm for L1, L2, and L5 carrier phases, respectively.

For aircraft and ships navigating en route, multipath is not typically considered the primary source of measurement errors because, in these cases, few-hundred-meter positioning errors are acceptable. Also, the integrity of navigational error information is more important than its value. For all applications where any form of differential correction is not required, the multipath phenomenon does not significantly affect the result. However, multipath becomes problematic in both differential code and phase positioning. Currently, this aspect is particularly considered when employing low-cost receivers and antennas, as they may not always be designed or computationally equipped to effectively mitigate the effects of multipath interference. Even though these types of receivers and antennas are increasingly used for precise measurements, the multipath phenomenon still has a greater impact on measurement results than in the case of professional receivers [7,8]. Performing differential positioning allows us to minimize the influence of most errors on positioning results. This includes the effects of the troposphere, ionosphere, and ephemeris data errors and receiver errors. However, this does not apply to multipath because it has a highly site-dependent characteristic that makes it time and space uncorrelated at different antenna locations [9,10]. Therefore, even for two receivers in close proximity, the effect of multipath will be different. This difference is mainly due to the short wavelength used in all GNSS systems [6]. In the case of carrier phase differential positioning, this error has two main effects. First, the multipath in the measured pseudorange increases the initial search space for correct ambiguities, extending the resolution time. Consequently, the accuracy of the vector solution between the reference station and the rover receiver is affected [11]. A number of methods have been developed to limit the influence of multipath on the measurement result. These methods can be divided into four categories [6]:

- Antenna placement;
- Antenna type;
- Receiver type;
- Measurement post-processing.

The easiest way to avoid multipath is to place the antenna in a place where there are no multipath signal sources nearby or with a very limited possibility of its occurrence [6,9,12]. This requirement is crucial for locating GBAS reference stations. However, this condition is troublesome and not always possible to meet due to factors such as urban environments or limited available space [13].

Another way to minimize the impact of multipath is to use a specially designed antenna. There are two main types of such antennas. The first one is a choke ring antenna consisting of one element inside a set of concentric rings. Due to their design and arrangement, these rings absorb electromagnetic waves that come from low or negative elevation angles [14–16]. The second type is the pinwheel antenna designed by NovAtel in the year 2000. This type of antenna consists of an array of 12 spiral slots surrounded by 11 concentric slot rings. It performs similarly to the choke ring antenna but is twice as small [17,18]. Nevertheless, due to their size, which is typically twice or once that of the L-band wavelength, both types of antennas are primarily used for reference stations, as their larger size may be impractical for rover receivers.

The third group of methods for minimizing the impact of multipath error is called “receiver type” and refers to the signal processing method inside the receiver. While receiver manufacturers are often hesitant to disclose details about their multipath mitigation methods, numerous such techniques are documented in the literature. The multipath limitation is related to the introduction of narrow correlator receiver architectures. Attention should be paid to the correlator schemes developed by Ashtech, the Strobe and Edge correlators [19]. Then, a year later, an enhanced Strobe correlator and Leica’s designed correlator were presented [20,21]. Later, super-resolution concepts were used to detect and minimize multipath [22]. Finally, receiver manufacturers most often used and still use a

double-delta correlator technique based on previous solutions [23]. Later on, a number of techniques based on the analysis of a number of correlators were developed and further investigated by researchers [24].

Despite the use of the methods above, the influence of the multipath phenomenon on the measurement results cannot be completely avoided. Therefore, several techniques for dealing with observations that have been contaminated by multipath have been developed. The approach to process such observations depends on whether the multipath mitigation algorithms are real-time or post-processing, and whether the receiver is stationary or kinematic. For kinematic applications, the simplest method is to apply to the weight of observations under the premise that the multipath value is inversely proportional to the satellite's elevation angle [6]. Methods based on signal-to-noise ratio analysis or code-to-noise ratio values were also developed [3]. The following method is common for both kinematic and static applications. It involves using a linear combination to find observations contaminated by multipath. Usually, the difference between the raw pseudorange measurement and the carrier-smooth measurement or the difference between code and carrier measurement is used. As a result of this operation, one obtains a metric value, the sum of noise and multipath. Then, the change in positioning model weighting can be made to minimize the influence of contaminated observations on the positioning result [25–27]. For receivers located at reference stations, sidereal filtering is often used. This method is based on the assumption that multipath repeats for a given satellite every sidereal day [28–30].

The multipath phenomenon is a complex process. Despite strategies that function at the level of transmission and acquisition of GNSS signals and processing of observations, it is still impossible to exclude this error. In the case of precise satellite measurements, this applies to both rover receivers and reference stations. The authors of this article analyzed the change in pseudorange multipath error from the years 2010 to 2021 in the Polish network of permanent GNSS stations, ASG-EUPOS. The year 2010 can be considered the beginning of the network operation in its current form, although it should be noted that the ASG-EUPOS system was initiated in 2008. As part of this research, 101 stations in the network were analyzed. Two computational strategies were adopted to determine the multipath: Code-Minus-Carrier (CMC) [25,31] and pseudorange multipath observable (MP) [32–34]. Both strategies are linear combinations of code and carrier GNSS observables. The computational methodology is described in detail in the next section. All available observation files from a given year were used for the study. The results of approximately 72,000 (30 s) RINEX files were analyzed, counting the results of the mentioned linear combinations for each epoch for each satellite. Such large data sets in the multipath context in the ASG-EUPOS network have not been analyzed yet. ASG-EUPOS is often used for RTK (real-time kinematic) and static positioning. In the assumed positioning methods, multipath can significantly impact the positioning algorithms' performance. The conducted research allows us to determine how the characteristics of this phenomenon have changed at ASG-EUPOS stations over the last decade. The authors wanted to check whether possible environmental changes around the reference stations affected the magnitude of the multipath error. Additionally, it was checked as to whether the changed generation of the receivers significantly impacted the multipath error. Studying the characteristics of the multipath error is one of the trends that modern geodesy deals with. The results of the analyses performed are important for geodynamic research in Poland. Due to its variable characteristics, multipath can significantly degrade the accuracy and reliability of positioning results. Reference stations of the studied network are used to determine the movements of the Earth's crust. Knowing the changes in multipath characteristics can influence the way of analyzing the time series used to calculate the station's speed and trend. This has a major impact on stations located in geologically stable areas where trend values are of several millimeters per year.

2. Materials and Methods

To determine the multipath value at ASG-EUPOS network stations, two computational strategies were employed. The first strategy utilized the observable values on the L1 carrier to calculate the Code-Minus-Carrier (CMC1) linear combination. The second strategy involved utilizing measurements on L1 and L2 carriers to determine the Multipath Pseudorange Observable combinations (MP1, MP2).

2.1. Code-Minus-Carrier Combination

The Code-Minus-Carrier (CMC) linear combination is employed based on the premise that multipath interference has a more pronounced impact on code measurements compared to phase measurements. As previously mentioned, multipath error values in pseudo-range measurements can reach several meters. Conversely, the maximum multipath error for phase measurements will not exceed 6.5 cm [4–6]. Therefore, a significant difference between the two values indicates a multipath effect. The subtraction of the measured quantities will eliminate receiver clock delay, satellite clock delay, tropospheric delay, and geometric distance. The CMC combination will have the following form:

$$CMC = p - \varphi\lambda = 2I + (M_p - M_\varphi) + (e - \epsilon) - N\lambda \quad (1)$$

where

- p —pseudorange measurement;
- φ —carrier-phase measurement;
- I —ionospheric delay;
- M_p —pseudorange multipath error (from several centimeters to few meters value);
- M_φ —carrier-phase multipath error (max 6.4 cm for L5 carrier);
- e —pseudorange noise (few centimeter value);
- ϵ —carrier-phase noise (sub-millimeter value);
- $N\lambda$ —carrier-phase range integer ambiguity.

Both the value of carrier-phase noise (ϵ) and the carrier-phase multipath (M_φ) can be neglected in further consideration because they are at least two orders of magnitude lower than in the case of their pseudorange measurement equivalents [6,35]. Consequently, the CMC combination equation takes the following form:

$$CMC \approx 2I + M_p + e - N\lambda \quad (2)$$

Referring to Equation (2), the determination of pseudorange multipath value necessitates the elimination or minimization of doubled ionospheric delay and the integer carrier-phase ambiguity. Both of these values can be regarded as either constant or partially constant due to their characteristics and behaviors over time. The carrier-phase integer ambiguity (N) value for a given satellite can be treated as constant, as the tests were conducted using static receivers, where this value remains unchanged. Prior to conducting the tests, measurement data underwent preprocessing to identify and correct cycle slips. The value of the ionospheric delay (I) can be treated as slowly varying during mild and moderate ionospheric conditions. Therefore, a filter was applied to account for the time correlation of the ionosphere within the range of 5 to 30 min [36,37]. Therefore, both of these values were treated as biases when determining the pseudorange multipath [6,38,39]. The SMA filter (Simple Moving Average) was used to eliminate both of these quantities. This filter assumes that the average value \overline{CMC} will be subtracted from each CMC value in the set. The \overline{CMC} value is calculated based on the equal number (k -samples) of data on either side of a CMC value. The method has been previously used in similar applications [27,39,40]. For the Code-Minus-Carrier combination, a number of k samples had to be selected to correspond to the period of change of the ionospheric delay (up to ± 15 min from the center CMC value). Then, the calculated average will take the following form:

$$\overline{CMC} = \frac{\sum_{i=-k}^k CMC_i}{2k + 1} \quad (3)$$

Finally, the value of multipath is obtained in the form of

$$CMC_{res} = CMC - \overline{CMC} = M_p + e + e_{res}, \quad (4)$$

where e_{res} is a residual error due to the removal of the ionosphere and integer ambiguity.

2.2. Pseudorange Multipath (MP) Observable Combination

Pseudorange multipath (MP) observable is a linear combination algorithm designed for dual frequency receivers. It assumes the use of dependencies between signals to determine the influence of multipath on the measurement results. Pseudorange multipaths MP_1 and MP_2 can be estimated according to the following equations [41–45]:

$$MP_1 = P_1 - \left(1 + \frac{2}{\alpha - 1}\right)\lambda_1\varphi_1 + \left(\frac{2}{\alpha - 1}\right)\lambda_2\varphi_2, \quad (5)$$

$$MP_2 = P_2 - \left(\frac{2\alpha}{\alpha - 1}\right)\lambda_1\varphi_1 + \left(\frac{2\alpha}{\alpha - 1} - 1\right)\lambda_2\varphi_2. \quad (6)$$

where

- MP_1, MP_2 —estimates of pseudorange multipath error [m];
- P_1, P_2 —pseudorange code measurement [m];
- λ_1, λ_2 —carrier wavelengths [m];
- φ_1, φ_2 —carrier—phase observable [cycles];
- f_1 and f_2 carrier frequency [Hz];
- $\alpha = (\frac{f_1}{f_2})^2$.

Resulting pseudorange multipath values (MP_1, MP_2) are contaminated with pseudorange measurement noise and instrumental delays (e), a constant component associated with phase ambiguities (B_1, B_2) and a component associated with carrier phase multipath ($m_{\varphi 1}, m_{\varphi 2}$) [5,45]:

$$MP_1 = M_{P1} - m_{\varphi 1} + e + B_1, \quad (7)$$

$$MP_2 = M_{P2} - m_{\varphi 2} + e + B_2. \quad (8)$$

As in the case of the CMC combination, these values can be considered constant until a cycle slip occurs. As mentioned earlier, after data preprocesing, it can be assumed that the data did not contain cycle slips. Therefore, the SMA filter was used with the same number of k-samples. Finally, the Multipath Pseudorange Observable values are obtained [33]:

$$MP_1 = mp_1 - \overline{mp_1}, \quad (9)$$

$$MP_2 = mp_2 - \overline{mp_2}. \quad (10)$$

3. Results

The research was carried out on the data from the network of permanent GNSS stations ASG-EUPOS. Data from 101 stations that existed in 2010 and 2021 were used. All available RINEX observation files were used for the calculations; for most stations, there were 365 files per year. Both Code-Minus-Carrier (CMC) combinations and Multipath Pseudorange (MP) observable combinations were used for multipath detection. Measurements with an interval of 30 s for satellites located above the 15° elevation angle were used. Phase measurement on the L1 carrier and C/A code pseudorange were used to calculate the CMC combination. In the case of the MP combination, the L1 and L2 carrier phase measurements and the C/A and P pseudoranges were used, respectively.

3.1. Code-Minus-Carrier L1 Analyses

As part of the CMC analyses, daily mean values of the Code-Minus-Carrier linear combination were determined for all available satellites. For the majority of stations, 365 average daily solutions were obtained. The statistical analysis of the obtained data is presented as a box plot. The results of the analyses conducted for 2010 are illustrated in Figures 1 and 2.

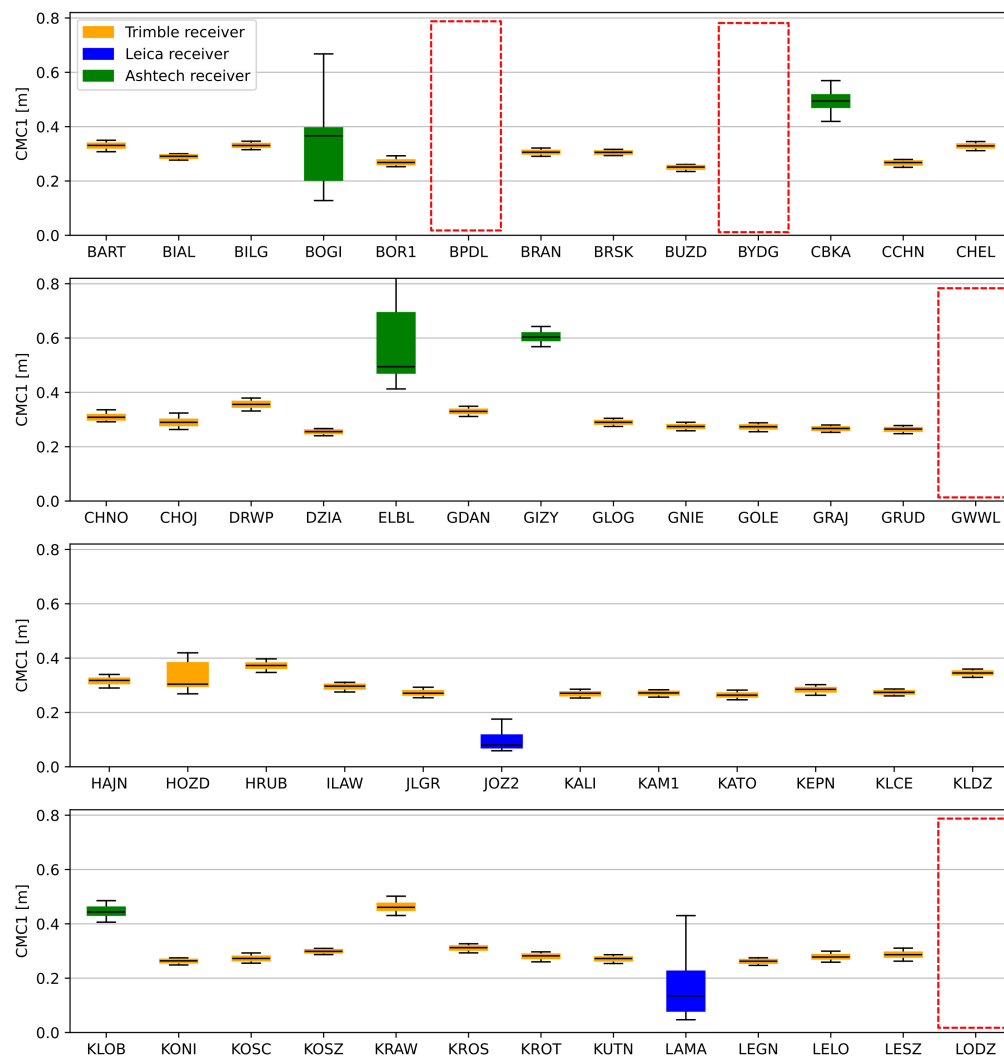


Figure 1. Annual statistics for 2010 of the Code-Minus-Carrier linear combination for the group of reference stations of the ASG-EUPOS system (BART–LODZ). Red box—station with very high CMC value.

In these figures, colors such as orange, blue, and green represent the types of receiver and antenna sets utilized at individual stations. In 2010, the majority of the sets consisted of Trimble (orange) devices, with 88 reference stations equipped with them. However, nine stations exhibited average CMC values that significantly surpassed the acceptable thresholds. These stations are marked with red rectangles (BPDL, BYDG, GWYL, LODZ, NODW, REDZ, SWKI, USDL, and ZYWI) in Figures 1 and 2. The results from these stations are further depicted in Figure 5. Excluding these nine stations, a noticeable consistency in the value and range of results is observed for most Trimble devices. The RMS values obtained there averaged 0.29 m, with a standard deviation of 0.01 m. Additionally, four Leica (blue) sets and six Ashtech (green) devices were installed. Although Leica results exhibit lower average RMS values compared to Trimble sets, they display a wider spread

(mean RMS value of 0.13 m with a standard deviation of 0.07 m). Ashtech receivers showed the highest RMS average CMC value and a distribution similar to Leica sets (mean CMC RMS value of 0.52 m with a standard deviation of 0.04 m).

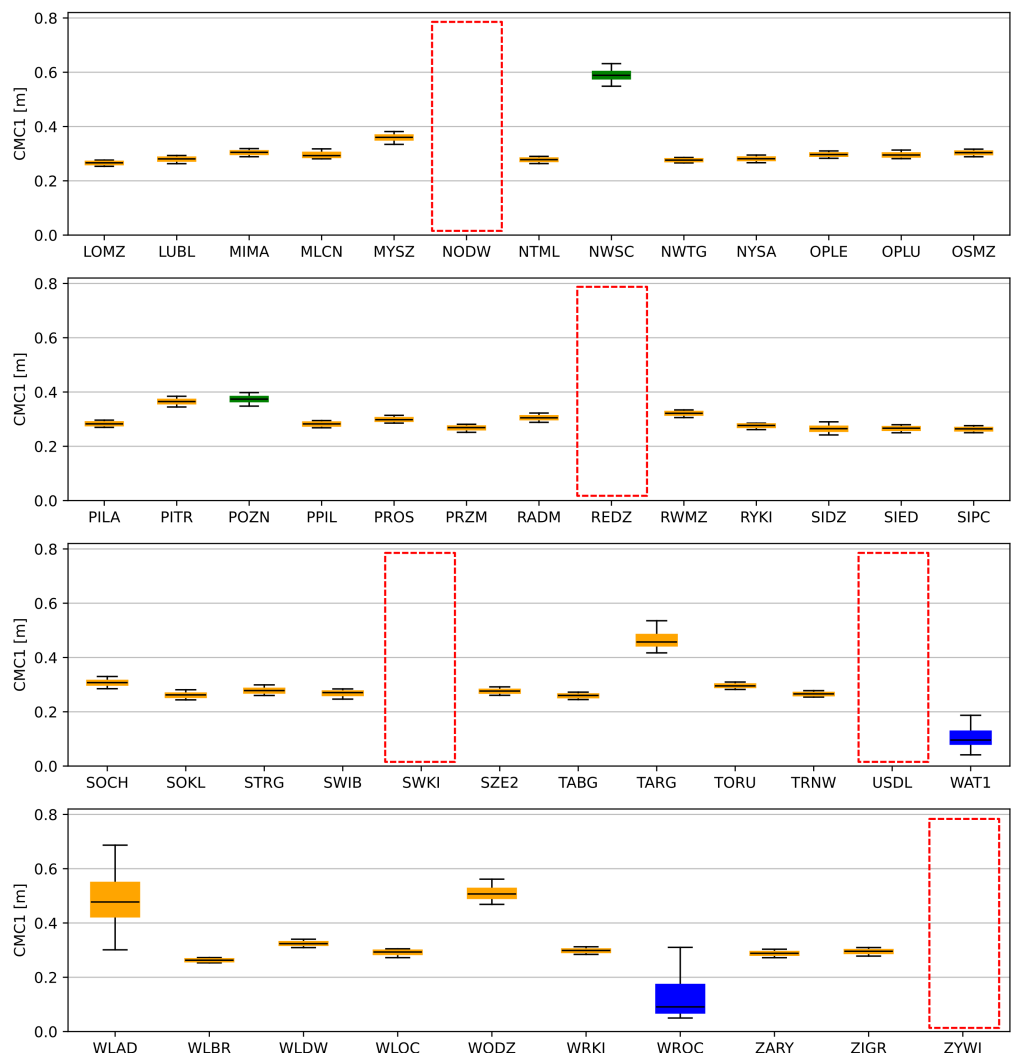


Figure 2. Annual statistics for 2010 of the Code-Minus-Carrier linear combination for the group of reference stations of the ASG-EUPOS system (LOMZ-ZYWI). Red box—station with very high CMC value.

The results of the analyses carried out for 2021 are presented in Figures 3 and 4. In these figures, the colors orange, blue, and green represent the various types of receiver and antenna sets utilized at individual stations. Leica sets are mounted at 60 stations, Trimble sets are installed at 38 stations, and a JAVAD receiver is installed at the BOGI station. The average multipath RMS value for the entire network was 0.21 m with a standard deviation of 0.03 m. The average RMS value for reference stations equipped with Leica sets was 0.14 m, while for stations with Trimble sets the value was 0.33 m. However, based on the analysis of data in Figures 3 and 4, it can be concluded that the data from the Trimble receivers had a smaller spread. For Leica sets, a similar pattern to that in the case of observations from 2010 is observed. Upon analyzing the statistical data, it becomes evident that several stations exhibit an average multipath value exceeding twice the network's overall average. These stations are BIAL, BRSK JOZ2, RYKI, NWSC, WAT1, and WIEL. Such statistical data may suggest the need for a deeper analysis.

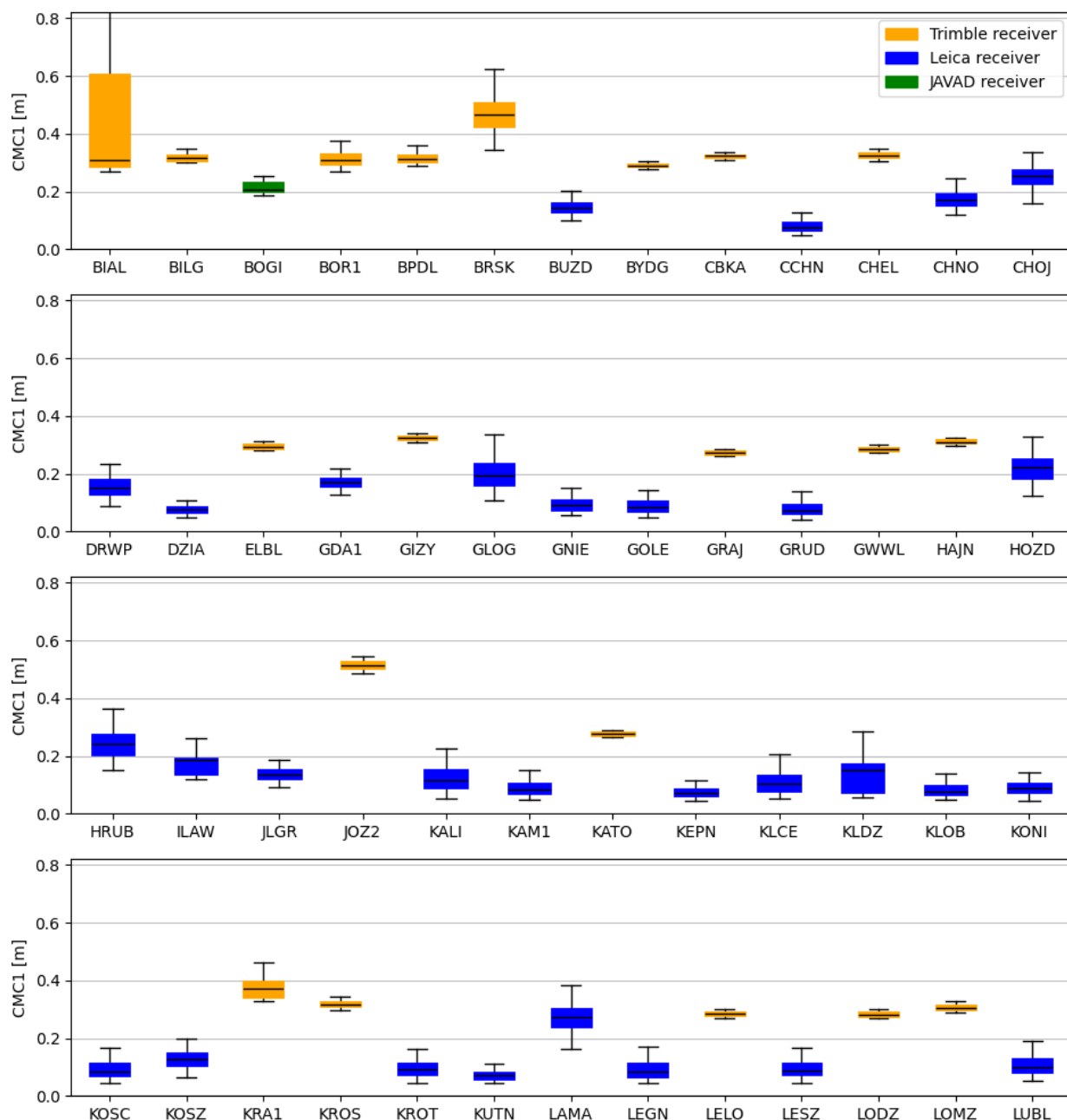


Figure 3. Annual statistics for 2021 of the Code-Minus-Carrier linear combination for the group of reference stations of the ASG-EUPOS system (BIAL-LUBL).

Comparing the collections from 2010 and 2021, it can be noticed that in 2021 the use of sets from the same manufacturer did not significantly change the characteristics of the multipath. This can be observed, for example, at station KROS. In 2010, it was equipped with a Trimble NETRS receiver and TRM41249.00 antenna set, which was changed to a Trimble NETR9 receiver and TRM159900.00 antenna set. The mean CMC value in 2021 remained at a similar level to that of 2010. Similar situations occur in the cases of stations BILG, BOR1, GRAJ, HAJN, LELO, MIMA, NWT1/NWTG, OSMZ, SOKL, TRNW, and WODZ/WOD1. Changing receivers to Leica devices decreased the average CMC values, although the distribution of results appears to be more pronounced with Leica sets. Removal of Ashtech receivers notably reduced multipath values at all stations (BOGI, CBKA, ELBL, GIZY, KLOB, NWSC, and POZN). At these reference stations, the average CMC RMS increased from 10% to 50%. As mentioned earlier, in 2010, nine stations were

identified for which the calculated mean RMS values of the Code-Minus-Carrier linear combination had significant values (Figure 5).

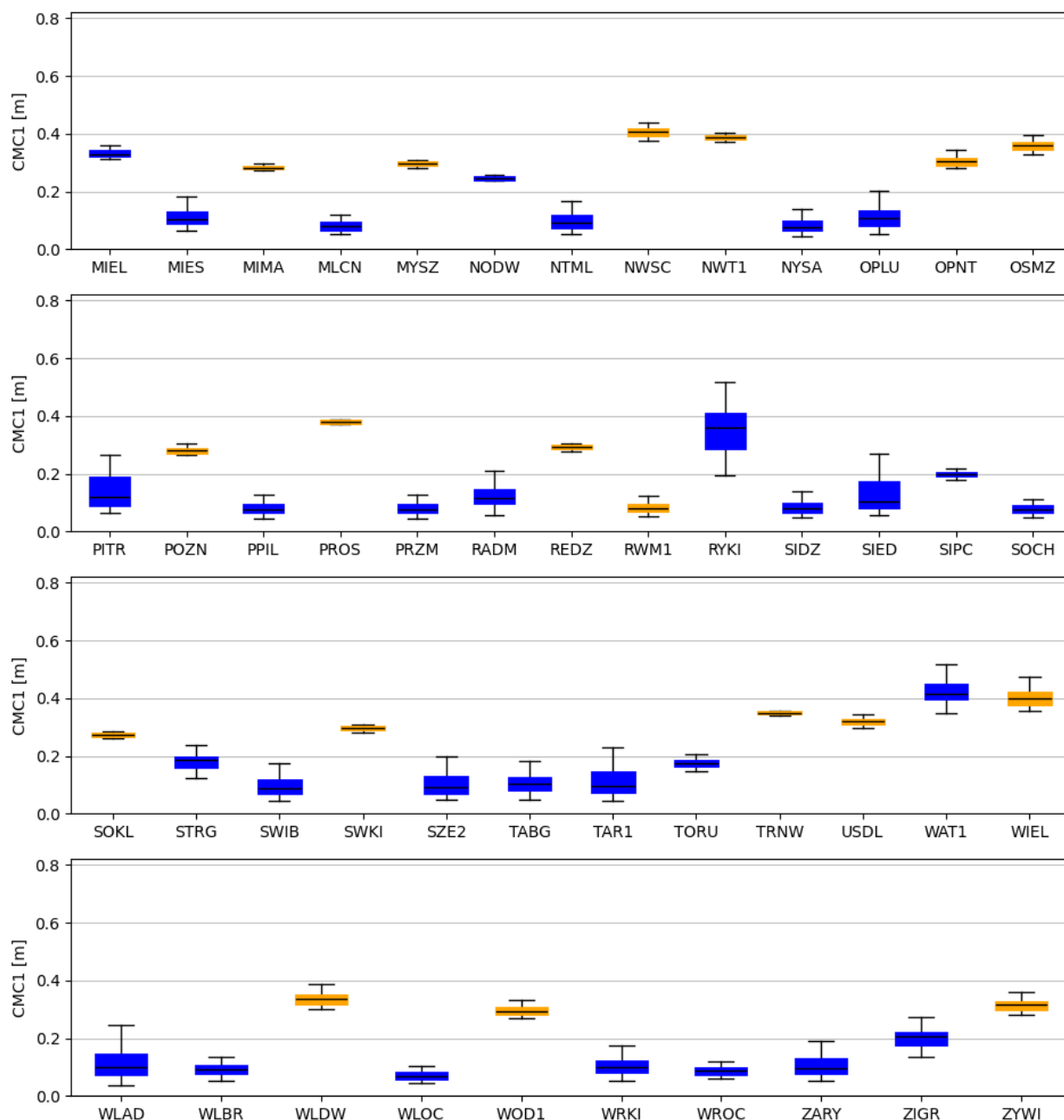


Figure 4. Annual statistics of the Code-Minus-Carrier linear combination for the group of reference stations of the ASG-EUPOS system (MIEL-ZYWI) in 2021.

In 2010, the selected stations were characterized by very high mean RMS values of the Code-Minus-Carrier linear combination. They oscillated around values from 2.25 m (NODW) to 3.00 m (ZYWI). The highest CMC values exceeded 4.00 m. Such multipath characteristics could influence the results of differential positioning using observations from these stations. As can be seen in 2021 (after changing the receiver and antenna sets), the characteristics of the multipath phenomenon do not differ from the average values observed in the entire network.

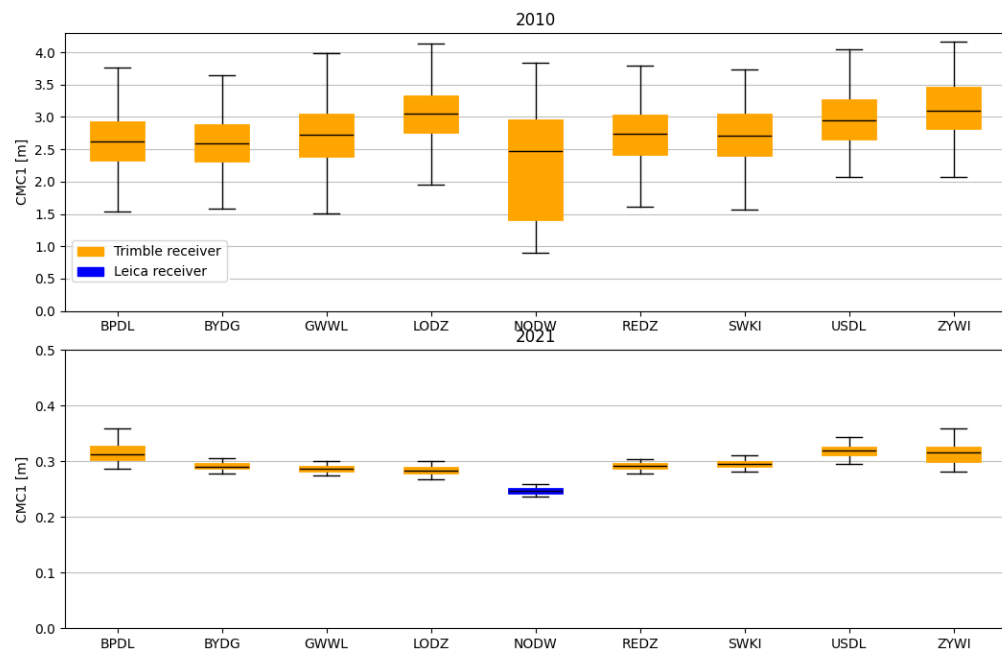


Figure 5. Annual statistics of the Code-Minus-Carrier linear combination for nine selected stations in 2010 and 2021.

3.2. Pseudorange Multipath Observable MP₁ MP₂ Analyses

As mentioned earlier, the second part of the research consisted of analyzing the results of linear MP combinations using L1 and L2 carrier frequencies. Daily mean values were determined for all available satellites above 15° elevation angle. For most stations, 365 average daily solutions were obtained. The results of the tests are presented as graphs of MP1 versus MP2 values for each station.

The results of the analyses carried out for 2010 are presented in Figure 6. The left part of Figure 7 shows the results from all analyzed stations. On the right side is an approximation of the distribution of MP1 vs. MP2 errors for the stations in the red rectangle (limit value 0.60 m). The results from the four Leica sets have the lowest values, oscillating from 0.10 m to 0.30 m for both combinations. The results from the six Ashtech sets have the highest RMS values on average, oscillating above 0.40 m. Most of the results from the Trimble sets are clustered in the 0.25 m to 0.40 m range for both the MP1 and MP2 combinations. As in the case of the analysis of the Code-Minus-Carrier linear combination, nine stations were characterized by very high average RMS values for both combinations. They oscillated from 2.46 m and 2.48 m for MP1 and MP2, respectively (NODW), to 3.26 m and 3.28 m for MP1 and MP2, respectively (SWKI). Except for the REDZ station (for which there were not enough observations on the L2 carrier), this is the same group of stations that was selected during the CMC analysis. Such multipath characteristics influenced the results of differential positioning using observations from these stations. The analysis in the next chapter will be devoted to these nine stations.

The analyses conducted for the year 2021 are presented in Figure 7. The left part of Figure 7 shows the results from all analyzed stations, while the right side depicts an approximation of the distribution of MP1 vs. MP2 errors for stations within the red rectangle (with a limit value of 0.60 m). In 2021, the average RMS values for MP1 and MP2 linear combinations were more symmetrical than in 2010. However, analogies can be noticed in the distribution of errors due to the used receiver sets. The study's results allow for drawing similar conclusions as in the case of the results from the CMC combination. Values achieved with Leica sets are slightly lower than those with Trimble sets. Twenty-eight stations equipped with Leica sets are below 0.35 m for both combinations, while only five Trimble sets can meet this criterion. For seven stations, the average RMS results are above 0.80 m (BART, BRSK, CHNO, CHOJ, HRUB, HOZD, and RYKI). The obtained results

correspond directly to the analysis performed in 2013 by Araszkiewicz and Szafranek [46]. In this publication, the authors used double-differenced ionosphere-free linear combination analysis to determine the phase multipath at ASG-EUPOS stations. Analogously to the current analysis, the HOZD, HRUB, and RYKI stations have higher analyzed RMS values. Therefore, in future studies, the observations from these stations will be examined more closely. The lowest values of MP1 and MP2 were achieved for the WROC station, which are 0.13 m and 0.14 m, respectively. Conversely, the station most susceptible to the multipath phenomenon is RYKI, with MP1 and MP2 values of 1.11 m and 1.26 m, respectively.

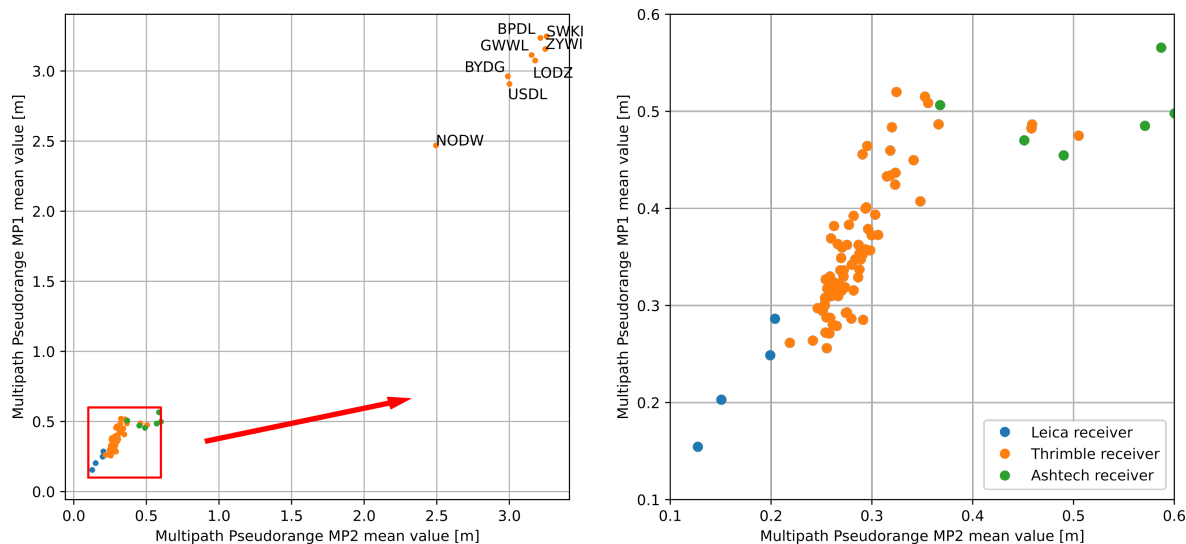


Figure 6. Annual statistics of the MP1 versus MP2 linear combinations for ASG-EUPOS reference stations in 2010.

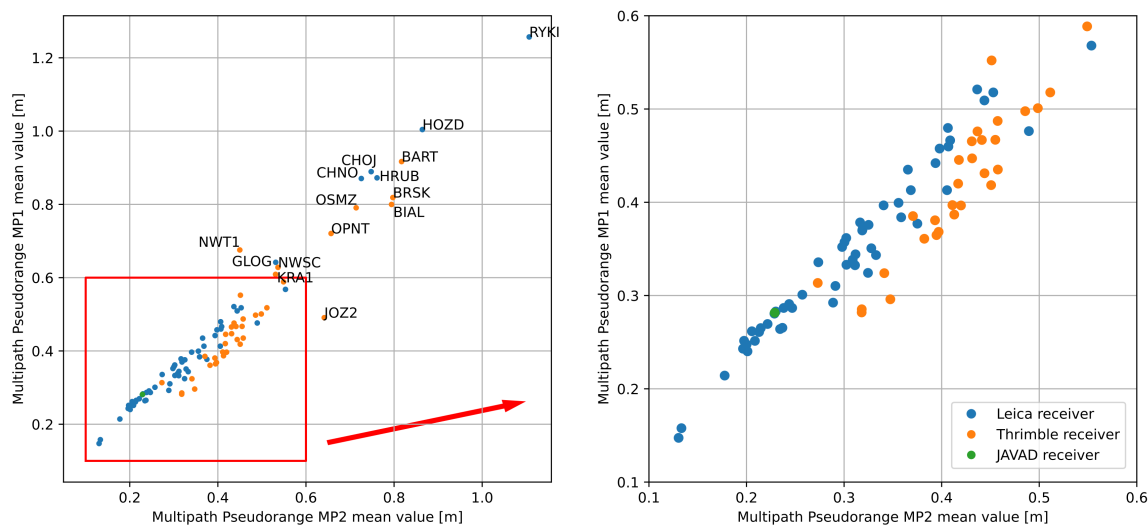


Figure 7. Annual statistics of the MP1 versus MP2 linear combinations for ASG-EUPOS reference stations in 2021.

3.3. Analysis of Data from Stations Characterized by Large RMS Averages for All Tested Combinations

This section provides a more detailed analysis of the results for BPDL, BYDG, GWWL, LODZ, NODW, REDZ, SWKI, USDL, and ZYWI (Figure 8—marked in bold). At these stations, there are significant differences in the results between 2021 and 2010. The results from 2010, in which the average values reach 3.0 m, suggest that the measurements at that time could significantly affect the positioning results using these stations. As a first analysis,

24 h sidereal maps have been created. Those maps would allow the identification of areas where all linear combinations had high results. The maps were separate for each linear combination of CMC1 and MP. The signals from satellites below 15 degrees elevation angle were excluded from the calculations because they are burdened with significant multipath and are often not used for differential positioning. Sidereal maps were created with an azimuth resolution of 0.5 degrees and elevation resolution of 0.5 degrees, and contained absolute values of determined quantities. Adjacent values belonging to one point of the map were averaged. The value adopted as the multipath combination threshold (T) was as follows:

$$T = 3\sigma, \quad (11)$$

where σ is the standard deviation of the whole set. Observations above this threshold were considered outliers. Sidereal maps for the problematic stations are depicted in Figures 9–11.

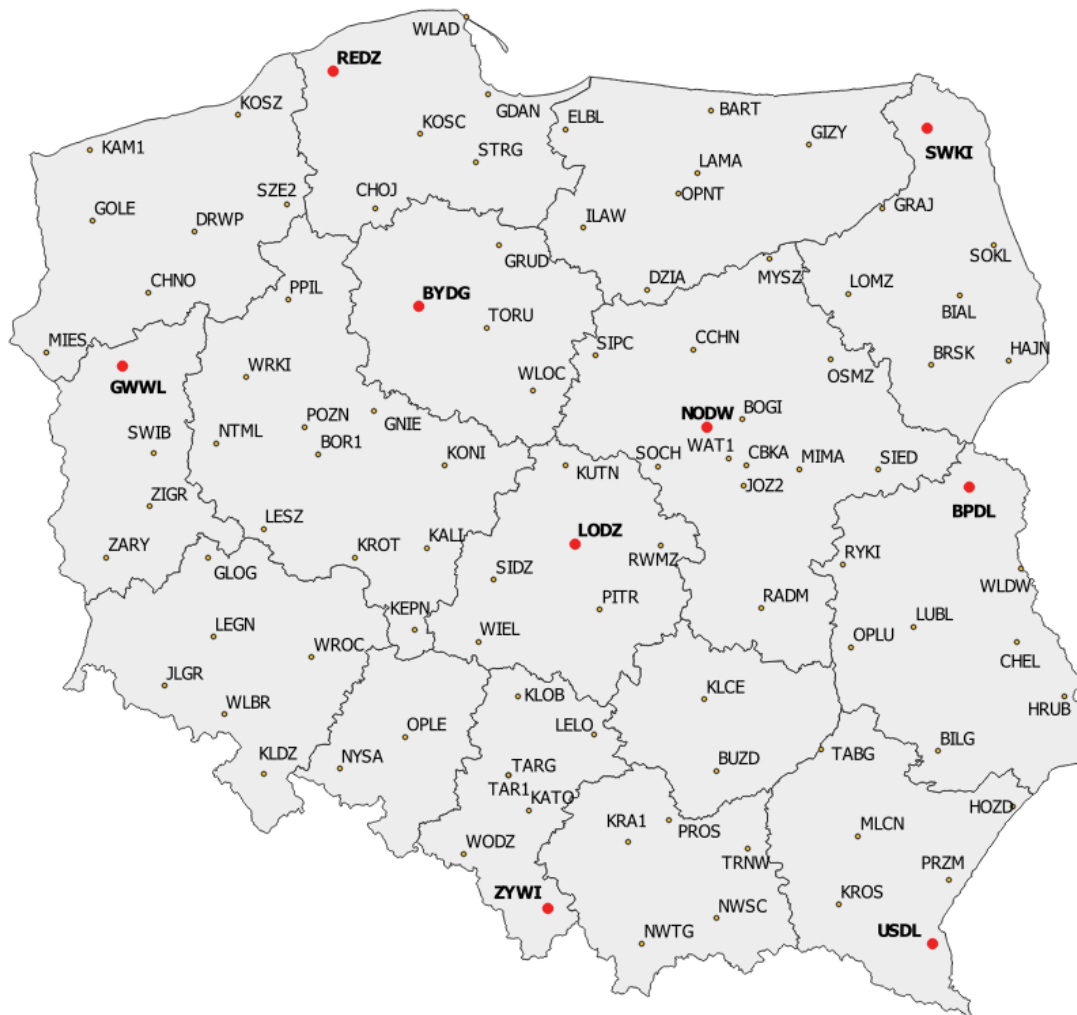


Figure 8. ASG-EUPOS reference stations map.

The sidereal maps were created based on the results from available observational files from 2010 (for example, 365 days for ZYWI station). Places where a high multipath value was repeated on each of the analyzed days are marked in red. The trajectory of the satellites is shown in blue. The maps for all the considered stations were very similar. It can be seen that the algorithm detected the influence of the multipath phenomenon in 90% of observations from a given station. Such a result is practically impossible, considering the antenna locations and the antenna models mounted on the reference stations. Therefore,

the authors decided to find the exact moment when the results from the reference stations decreased to acceptable levels. Since 2010, average daily RMS values have been determined for all problematic stations. In 2011, after DOY 143, all tested stations had an acceptable average RMS for all considered linear combinations (Figure 12).

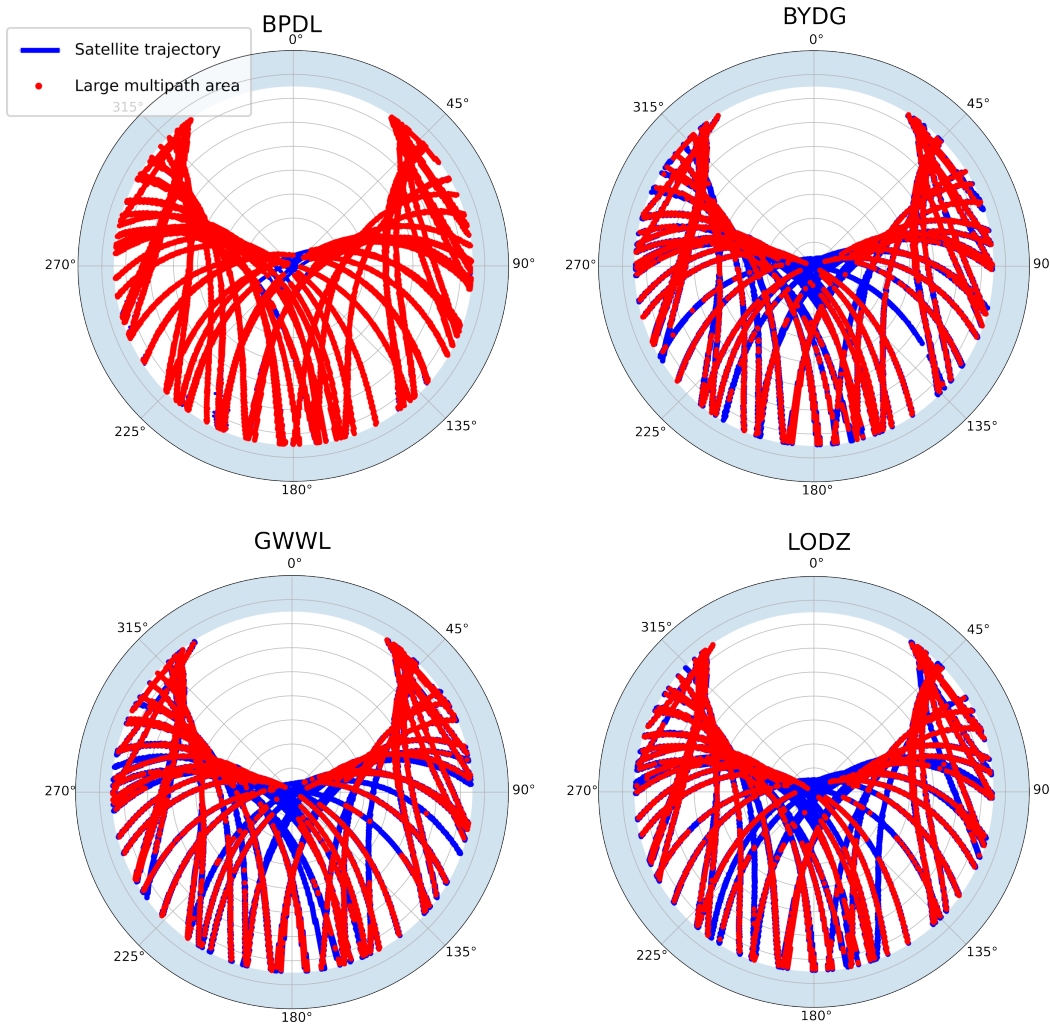


Figure 9. Mean 2010 sky plots with sidereal maps of BPDL, BYDG, GWWL, and LODZ stations.

Figure 12 depicts the time series of daily RMS values for the nine considered stations. In the case of all receivers, there was a significant change on day 143 of 2011. As can be seen in Figure 8, the stations are randomly distributed throughout the country; so, it is not possible for significant changes in the environment that would change the multipath statistics to occur at the same time. Therefore, the next step was to analyze the log files from the reference stations. These materials include, among others, information about the receivers, antennas, and the version of the software that was on the receiver. It was established that nine stations were the only ones with Nav 3.8/Boot 3.56 receiver software. On DOY 143, the receiver's firmware version was changed at those stations from Nav 3.8/Boot 3.56 to Nav 4.41/Boot 4.18, which significantly decreased the values of the tested linear combinations (CMC, MP1 MP2). Therefore, the authors conclude that the incorrect values of the tested linear combinations (CMC, MP1 MP2), high daily RMS, and average annual RMS result from improper operation or incorrect settings of the receivers located at the nine considered stations.

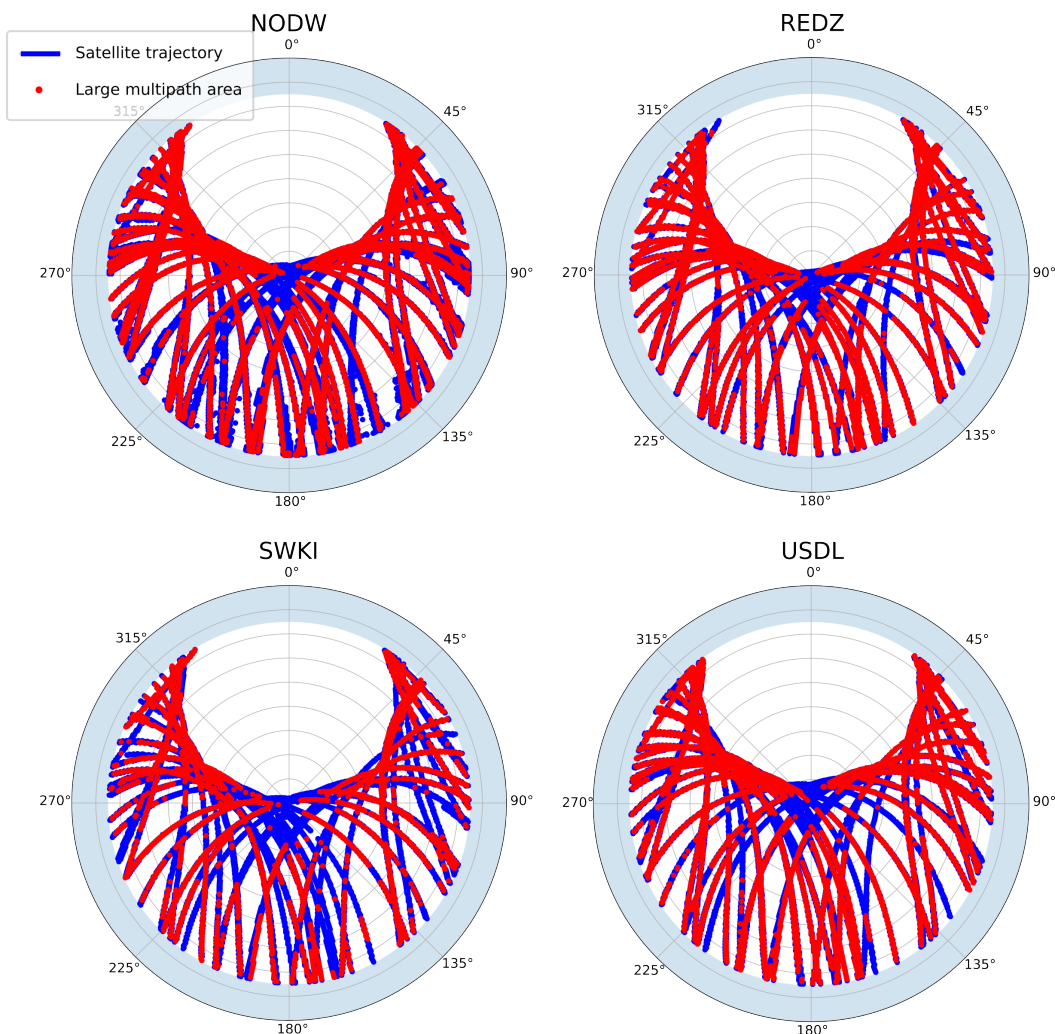


Figure 10. Mean 2010 sky plots with sidereal maps of NODW, REDZ, SWKI, and USDL stations.

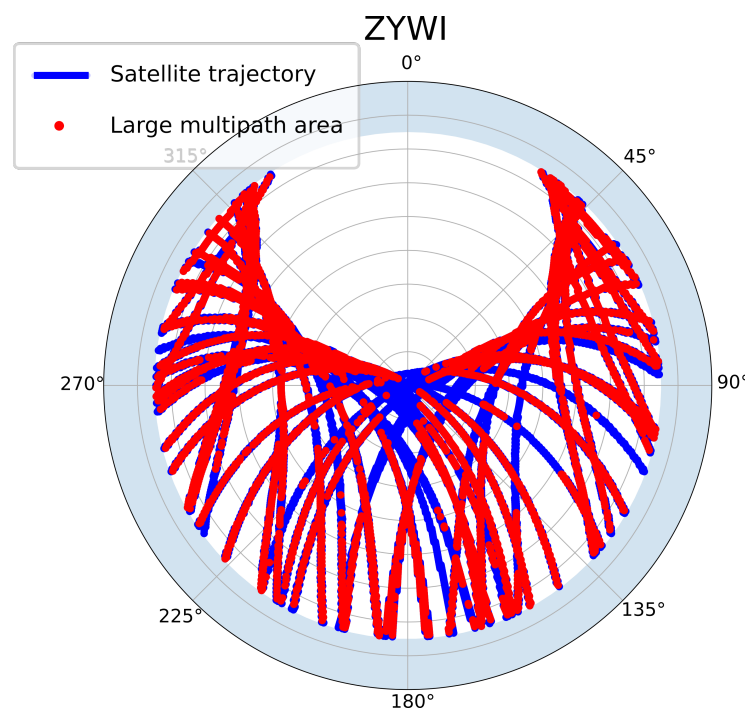


Figure 11. Mean 2010 sky plot with sidereal map of ZYWI station.

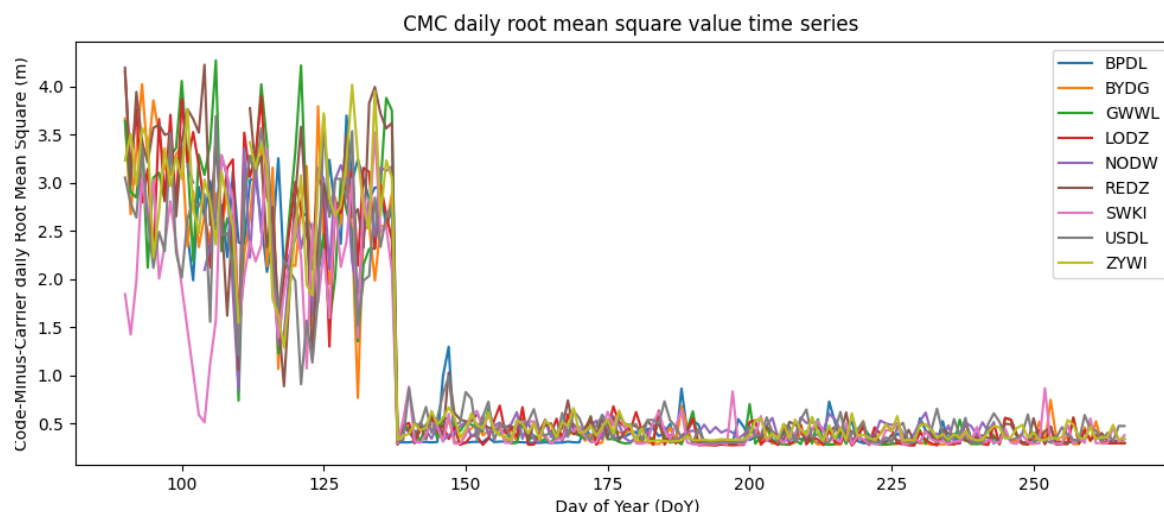


Figure 12. CMC RMS time series for the surveyed stations in 2011.

4. Discussion

This study conducted a comparative analysis of the impact of the multipath phenomenon on the results of GNSS measurements at ASG-EUPOS system reference stations between 2010 and 2021. The tests used the Code-Minus-Carrier linear combination at the GPS L1 frequency and pseudorange measurement linear combination at the L1 and L2 frequencies. Two methods were employed to determine the multipath impact, providing reference values and a comparative scale. In 2010, nine stations were detected for which the average results for all tested combinations exceeded 2.50 m. Additional analyses were performed for these stations and found that the reason for such high values was the improper operation of receivers with a specific firmware version. Consequently, the authors concluded that false multipath effects were detected due to firmware error or incorrect receiver configuration. The remaining analyses were conducted excluding these nine stations. In 2010, most of the receiver and antenna sets installed at ASG-EUPOS system stations were manufactured by Trimble, while in 2021, 60 percent of the sets came from Leica. Regardless of the considered year, it can be seen that the Trimble receivers are characterized as having about 0.15 m higher average values of every linear combination than those of the Leica receivers but they also have a lower standard deviation. These differences were directly reflected in the overall annual statistics for the analyzed periods. The average value of the CMC linear combination in 2010 was 0.30 m with a standard deviation of 0.01 m, whereas in 2021, these values stood at 0.21 m and 0.03 m, respectively. In 2021, the average CMC linear combination RMS value for the stations with Leica sets was 0.13 m, with a 0.07 m standard deviation. In 2010, only four stations were equipped with Leica sets, precluding accurate statistical analysis. However, it should be noted that the average RMS value was 0.14 m for these four stations. Analyses conducted on linear combinations MP1 and MP2 yielded very similar results. Notably, no significant increase in the multipath impact on measurement results was observed for any of the tested stations, indicating the absence of new multipath-causing objects in the vicinity of the stations. Based on the research, it can be concluded that the impact of the multipath error decreased between 2010 and 2021. This change mainly results from the applied technological solutions. However, the observed change is insignificant and will not increase the positioning quality. Although significant differences can obviously be observed at the nine stations that worked incorrectly in 2010 and in half of 2011. Given the prolonged incorrect operation of receivers at these nine stations, the authors recommend evaluating observation results after each firmware update. Future research endeavors are planned to assess the current state of multipath in the ASG-EUPOS network. Considering the network's utilization for modeling Earth's crust

movement, the authors intend to investigate carrier phase multipath, which is crucial for both real-time kinematic positioning (RTK) and precise point positioning (PPP).

Author Contributions: Conceptualization, D.T. and J.R.; methodology, D.T.; software, D.T.; validation, D.T., J.R. and R.P.-M.; formal analysis, R.P.-M.; investigation, D.T.; resources, R.P.-M.; data curation, D.T.; writing—original draft preparation, D.T.; writing—review and editing, J.R. and R.P.-M.; visualization, D.T.; supervision, J.R.; project administration, D.T.; funding acquisition, J.R. All authors have read and agreed to the published version of the manuscript.

Funding: This research received no external funding.

Data Availability Statement: The data presented in this study are available on request from the corresponding author. The data are not publicly available due to legal reasons.

Conflicts of Interest: The authors declare no conflicts of interest.

References

1. Groves, P.D. The PNT boom: Future trends in integrated navigation. *Inside GNSS* **2013**, *8*, 44–49.
2. Qin, H.; Xue, X.; Yang, Q. GNSS multipath estimation and mitigation based on particle filter. *IET Radar Sonar Navig.* **2019**, *13*, 1588–1596. [[CrossRef](#)]
3. Strode, P.R.; Groves, P.D. GNSS multipath detection using three-frequency signal-to-noise measurements. *GPS Solut.* **2016**, *20*, 399–412. [[CrossRef](#)]
4. Hofmann-Wellenhof, B.; Lichtenegger, H.; Collins, J. *Global Positioning System: Theory and Practice*; Springer Science & Business Media: Berlin/Heidelberg, Germany, 2012.
5. Robustelli, U.; Pugliano, G. Code multipath analysis of Galileo FOC satellites by time-frequency representation. *Appl. Geomat.* **2019**, *11*, 69–80. [[CrossRef](#)]
6. Teunissen, P.J.; Montenbruck, O. *Springer Handbook of Global Navigation Satellite Systems*; Springer: Berlin/Heidelberg, Germany, 2017; Volume 10.
7. Krzan, G.; Dawidowicz, K.; Paziewski, J. Low-cost GNSS antennas in precise positioning: A focus on multipath and antenna phase center models. *GPS Solut.* **2024**, *28*, 103. [[CrossRef](#)]
8. Paziewski, J. Multi-constellation single-frequency ionospheric-free precise point positioning with low-cost receivers. *GPS Solut.* **2022**, *26*, 23. [[CrossRef](#)]
9. Pelc-Mieczkowska, R.; Tomaszewski, D.; Bednarczyk, M. GNSS obstacle mapping as a data preprocessing tool for positioning in a multipath environment. *Meas. Sci. Technol.* **2019**, *31*, 015017. [[CrossRef](#)]
10. Smyrnaios, M.; Schn, S.; Liso, M.; Jin, S. Multipath propagation, characterization and modeling in GNSS. In *Geodetic Sciences-Observations, Modeling and Applications*; IntechOpen: Rijeka, Croatia, 2013; pp. 99–125.
11. Spilker, J.J., Jr.; Axelrad, P.; Parkinson, B.W.; Enge, P. *Global Positioning System: Theory and Applications, Volume I*; American Institute of Aeronautics and Astronautics: Reston, VA, USA, 1996.
12. Kavak, A.; Xu, G.; Vogel, W.J. GPS multipath fade measurements to determine L-band ground reflectivity properties. In Proceedings of the 20th NASA Propagation Experimenters Meeting, Fairbanks, AK, USA, 4–6 June 1996.
13. Rotondo, G.; Thevenon, P.; Milner, C.; Macabiau, C.; Felux, M.; Hornbostel, A.; Circiu, M.S. Methodology for determining Pseudorange noise and multipath models for a multi-constellation, multi-frequency GBAS system. In Proceedings of the 2015 International Technical Meeting of the Institute of Navigation, Dana Point, CA, USA, 26–28 January 2015; pp. 383–392.
14. Tranquilla, J.M.; Carr, J.; Al-Rizzo, H.M. Analysis of a choke ring groundplane for multipath control in global positioning system (GPS) applications. *IEEE Trans. Antennas Propag.* **1994**, *42*, 905–911. [[CrossRef](#)]
15. Kunysz, W. A three dimensional choke ring ground plane antenna. In Proceedings of the 16th International Technical Meeting of the Satellite Division of the Institute of Navigation (ION GPS/GNSS 2003), Portland, OR, USA, 9–12 September 2003; pp. 1883–1888.
16. Danskin, S.; Bettinger, P.; Jordan, T. Multipath mitigation under forest canopies: A choke ring antenna solution. *For. Sci.* **2009**, *55*, 109–116. [[CrossRef](#)]
17. Kunysz, W. High performance GPS pinwheel antenna. In Proceedings of the 13th International Technical Meeting of the Satellite Division of the Institute of Navigation (ION GPS 2000), Salt Lake City, UT, USA, 19–22 September 2000; pp. 2506–2511.
18. Kunysz, W. A Novel GPS Survey Antenna. In Proceedings of the 2000 National Technical Meeting of the Institute of Navigation, San Diego, CA, USA, 26–28 January 2000; pp. 698–705.
19. Garin, L.; van Diggelen, F.; Rousseau, J.M. Strobe & edge correlator multipath mitigation for code. In Proceedings of the 9th International Technical Meeting of the Satellite Division of the Institute of Navigation (ION GPS 1996), Kansas City, MO, USA, 17–20 September 1996; pp. 657–664.
20. Garin, L.; Rousseau, J.M. Enhanced strobe correlator multipath rejection for code & carrier. In Proceedings of the 10th International Technical Meeting of the Satellite Division of the Institute of Navigation (ION GPS 1997), Kansas City, MO, USA, 16–19 September 1997; pp. 559–568.

21. Hatch, R.R.; Keegan, R.G.; Stansell, T.A. Leica's code and phase multipath mitigation techniques. In Proceedings of the 1997 National Technical Meeting of the Institute of Navigation, Kansas City, MO, USA, 16–19 September 1997; pp. 217–225.
22. Weill, L.R. Application of superresolution concepts to the GPS multipath mitigation problem. In Proceedings of the 1998 National Technical Meeting of the Institute of Navigation, Long Beach, CA, USA, 21–23 January 1998; pp. 673–682.
23. Irsigler, M.; Eissfeller, B. Comparison of multipath mitigation techniques with consideration of future signal structures. In Proceedings of the 16th International Technical Meeting of the Satellite Division of the Institute of Navigation (ION GPS/GNSS 2003), Portland, OR, USA, 9–12 September 2003; pp. 2584–2592.
24. Paonni, M.; AVILA-RODRIGUEZ, J.A.; Pany, T.; Hein, G.W.; Eissfeller, B. Looking for an Optimum S-Curve Shaping of the Different MBOC Implementations. *Navigation* **2008**, *55*, 255–266. [[CrossRef](#)]
25. Ray, J.; Cannon, M.; Fenton, P. GPS code and carrier multipath mitigation using a multiantenna system. *IEEE Trans. Aerosp. Electron. Syst.* **2001**, *37*, 183–195. [[CrossRef](#)]
26. Irsigler, M. Characterization of multipath phase rates in different multipath environments. *GPS Solut.* **2010**, *14*, 305–317. [[CrossRef](#)]
27. Robustelli, U.; Pugliano, G. GNSS Code Multipath Short-time Fourier Transform Analysis. *Navig. J. Inst. Navig.* **2018**, *65*, 353–362. [[CrossRef](#)]
28. Wanninger, L.; May, M. Carrier-Phase Multipath Calibration of GPS Reference Stations. *Navigation* **2001**, *48*, 112–124. [[CrossRef](#)]
29. Choi, K.; Bilich, A.; Larson, K.M.; Axelrad, P. Modified sidereal filtering: Implications for high-rate GPS positioning. *Geophys. Res. Lett.* **2004**, *31*. [[CrossRef](#)]
30. Zaminpardaz, S.; Teunissen, P.J.; Nadarajah, N. IRNSS stand-alone positioning: First results in Australia. *J. Spat. Sci.* **2016**, *61*, 5–27. [[CrossRef](#)]
31. Braasch, M.S. Isolation of GPS multipath and receiver tracking errors. *Navigation* **1994**, *41*, 415–435. [[CrossRef](#)]
32. Defraigne, P.; Bruyninx, C. On the link between GPS pseudorange noise and day-boundary discontinuities in geodetic time transfer solutions. *GPS Solut.* **2007**, *11*, 239–249. [[CrossRef](#)]
33. Hilla, S.; Cline, M. Evaluating pseudorange multipath effects at stations in the National CORS Network. *GPS Solut.* **2004**, *7*, 253–267. [[CrossRef](#)]
34. Abou Galala, M.; Kaloop, M.R.; Rabah, M.M.; Zeidan, Z.M. Improving precise point positioning convergence time through TEQC multipath linear combination. *J. Surv. Eng.* **2018**, *144*, 04018002. [[CrossRef](#)]
35. El-Rabbany, A. *Introduction to GPS: The Global Positioning System*; Artech House: London, UK, 2002.
36. Mannucci, A.; Iijima, B.; Wilson, B. Wide area ionospheric delay corrections under ionospheric storm conditions. In Proceedings of the 1997 National Technical Meeting of the Institute of Navigation, Santa Monica, CA, USA, 14–16 January 1997; Volume 1, pp. 871–882.
37. Krypiak-Gregorczyk, A.; Wielgosz, P.; Borkowski, A. Ionosphere model for European region based on multi-GNSS data and TPS interpolation. *Remote Sens.* **2017**, *9*, 1221. [[CrossRef](#)]
38. Jiang, Y.; Milner, C.; Macabiau, C. Code carrier divergence monitoring for dual-frequency GBAS. *GPS Solut.* **2017**, *21*, 769–781. [[CrossRef](#)]
39. Pirsiavash, A.; Broumandan, A.; Lachapelle, G.; O'Keefe, K. GNSS code multipath mitigation by cascading measurement monitoring techniques. *Sensors* **2018**, *18*, 1967. [[CrossRef](#)] [[PubMed](#)]
40. Zhang, Z.; Guo, F.; Zhang, X.; Pan, L. First result of GNSS-R-based sea level retrieval with CMC and its combination with the SNR method. *GPS Solut.* **2022**, *26*, 20. [[CrossRef](#)]
41. Estey, L.H.; Meertens, C.M. TEQC: The multi-purpose toolkit for GPS/GLONASS data. *GPS Solut.* **1999**, *3*, 42–49. [[CrossRef](#)]
42. Vázquez, G.E.; Bennett, R.; Spinler, J. Assessment of pseudorange multipath at continuous GPS stations in Mexico. *Positioning* **2013**, *2013*, 36358. [[CrossRef](#)]
43. Guo, J.; Li, G.; Kong, Q.; Wang, S.; Zong, G. On site pseudorange multipath effect on GPS surveying. In *Principle and Application Progress in Location-Based Services*; Springer: Berlin/Heidelberg, Germany, 2014; pp. 107–120.
44. Leick, A.; Rapoport, L.; Tatarnikov, D. *GPS Satellite Surveying*; John Wiley & Sons: Hoboken, NJ, USA, 2015.
45. Seepersad, G.; Bisnath, S. Reduction of PPP convergence period through pseudorange multipath and noise mitigation. *GPS Solut.* **2015**, *19*, 369–379. [[CrossRef](#)]
46. Araszkiewicz, A.; Szafranek, K. LC phase bias investigation of ASG-EUPOS stations. *Geod. Cartogr.* **2013**, *62*, 101–111. [[CrossRef](#)]

Disclaimer/Publisher's Note: The statements, opinions and data contained in all publications are solely those of the individual author(s) and contributor(s) and not of MDPI and/or the editor(s). MDPI and/or the editor(s) disclaim responsibility for any injury to people or property resulting from any ideas, methods, instructions or products referred to in the content.